https://doi.org/10.5194/egusphere-2026-1299
Preprint. Discussion started: 13 March 2026

First Continuous Aerosol Measurements at Testa Grigia at 3480 m asl: Aerosol Populations and Transport Dynamics in the Southern European Alps

Stefania Gilardoni[1], Annachiara Bellini[2], Paolo Bonasoni[3], Henri Diémoz[2], Christian Gencarelli[4], Angela Marinoni[3], Eros Mariani[5], Luigi Mazari Villanova[6], Bruno Neininger[7], Mattia Perilli[8], Michael Sprenger[9], Francesco Petracchini[6]

[1] Institute of Polar Sciences - National Research Council, Milan, Italy

[2] ARPA Valle d'Aosta, Saint-Christophe, Italy

[3] Institute of Atmospheric Sciences and Climate - National Research Council, Bologna, Italy

[4] Institute of Institute of Environmental Geology and Geoengineering - National Research Council, Milan, Italy

[5] Research Area Milano 1 - National Research Council, Milan, Italy

[6] Department of Earth System Science and Environmental Technologies - National Research Council, Rome, Italy

[7] MetAir AG, Menzingen, Switzerland

[8] Institute of Atmospheric Pollution - National Research Council, Rome, Italy

[9] Institute for Atmospheric and Climate Science, ETH Zurich, Zurich, Switzerland

Correspondence to: Stefania Gilardoni (Stefania.gilardoni@cnr.it)

Abstract High-elevation observatories are crucial for monitoring atmospheric aerosols, which play a key role in the climate system due to their effects on radiation, cloud, and snow albedo. We present the first measurements of aerosol size distribution and absorption coefficient at a 1-hour time resolution collected at the Testa Grigia Observatory (3,480 m asl) in the Italian Alps. This dataset spans from September 2021 to May 2023. We identified three distinct aerosol population types reaching the observatory, reflecting distinct transport pathways. The coarse particle population is indicative of long-range transport air masses from Sahara. Conversely, the fine particle population is linked to mesoscale circulations and boundary layer dynamics (from the Po Valley and local alpine valleys), and broader continental flows. Finally, periods of generally low particle number correspond to the influence of clean air from the free troposphere and the Mediterranean basin. The upper bound of the frequency of boundary layer influence is equal to 28%. Conversely, Sahara Dust Events (SDE), identified as periods characterized by coarse aerosol population transported from the Sahara region, are observed for 6% of the time. These events are predominantly recorded during spring and early summer and show strong correspondence with reanalysis data provided by CAMS (Copernicus Atmosphere Monitoring Service) ensemble model. The seasonal variability of PM10 concentration associated to SDE is explained by the variability to dust emission regions, dust mobilization over source region, and efficiency of dust transport mechanisms.

1. Introduction

Atmospheric aerosols play a crucial role in the climate system due to their ability to absorb and scatter shortwave radiation and to their impact on cloud microphysical properties. Aerosol-radiation and aerosol-cloud interaction represent significant sources of uncertainty in climate models (Flato et al., 2014; Fyfe et al., 2021; Regayre et al., 2018). Notably, the radiative forcing resulting from aerosol-cloud interaction stands as one of the primary contributors to the variability in climate sensitivity estimates and the associated radiative forcing uncertainty has not decreased during the last four

https://doi.org/10.5194/egusphere-2026-1299
Preprint. Discussion started: 13 March 2026

IPCC cycles (Houghton et al., 2001; Chen et al., 2021). To effectively reduce the uncertainty surrounding aerosol radiative forcing, it is essential to obtain high-quality observational data that can accurately constrain the microphysical properties of aerosols and map their vertical distribution throughout the atmosphere (Seinfeld et al., 2016).

Understanding and quantitatively describing aerosol properties at high elevations is essential for assessing their radiative impact and climate feedback. First, the vertical distribution of aerosols influences the atmospheric thermal profile (Ramanathan and Carmichael, 2008; Wilcox et al., 2016) and controls the availability of particles that can condense water to form cloud droplets or nucleate ice crystals at high altitudes (Rosenfeld et al., 2008; Kanji et al., 2017; Burrows et al., 2022). Second, aerosols in the free troposphere have a longer atmospheric lifetime compared to those in the lower troposphere due to limited removal rate (Williams et al., 2002) . The higher wind speeds in the free troposphere facilitate long-distance transport, extending the impact of aerosols on climate and air quality far from their emission sources (Laing et al., 2016; Igel et al., 2017). Finally, in mountain regions, light-absorbing aerosols at high elevations can deposit on snow, accelerating snowmelt and altering planetary albedo (Skiles et al., 2018; PöRtner et al., 2019).

Mountaintop observatories represent an essential tool for filling knowledge gaps on aerosol at high elevations (Andrews et al., 2011; Collaud Coen et al., 2020). Mountain observatories allow for continuous monitoring of several aerosol variables, enabling the analysis of daily (Nyeki et al., 1998a; Shaw, 2007), seasonal (NicoláS et al., 2018; Gallagher et al., 2011; Singh et al., 2020; Sellegri et al., 2010), and long-term atmospheric composition changes at high elevations (Collaud Coen et al., 2013). Collaud Coen et al. (2020) investigated long-term trend in aerosol optical properties across 54 observatories, including 16 mountain sites. At these sites, the manuscript reports a decreasing trend in aerosol absorption and scattering coefficient during the last 10 to 20 years in Europe and North America, reflecting the decrease in anthropogenic aerosol and aerosol precursor emissions, not just at local scale but at regional and hemispheric scale.

Furthermore, observatories located at high elevations provide a unique opportunity to sample the free troposphere, allowing for the investigation of long-range transport processes. For instance, measurements of particle number size distribution at Monte Cimone, in the northern Apennines, allowed the analysis of long-term impact of Saharan dust transport events over distances greater than 1000 km and revealed that the frequency of dust transport days in the study region ranged from 15% to 20% over the past 20 years, with no significant trend observed over time (Vogel et al., 2025; Duchi et al., 2016). Similarly, aerosol optical properties measured at Jungfraujoch, in the western Alps, indicated that Sahara dust transport episodes reached the Alps between 30 and 150 times per year during the last 23 years (2001-2024) (Collaud Coen et al., 2025). Additionally, the long-range transport of wildfire plumes occurring in the upper troposphere and lower stratosphere at hemispheric scale can also be detected, with in-situ measurements providing new insights into aerosol composition, microphysical processes, and the effects of atmospheric aging (Masoom et al., 2025; Dzepina et al., 2015; Laj et al., 2009).

High-elevation observatories are spatially more representative than boundary layer measurements, and this makes these sites extremely useful for the evaluation of aerosol model performance and for the validation of satellite products (Laj et al., 2009; Gilardoni et al., 2011).

The northern edge of the European Alps is home to three mountaintop observatories that monitor continuously aerosol microphysical and optical properties at high time resolution at elevations ranging from 2,600 m to 3,600 m: Jungfraujoch, situated on the northern edge of the Swiss Alps at an altitude of 3,580 m above sea level (Nyeki et al., 1998a), the Environmental Research Station Schneefernerhaus, located at the Zugsptize mountain on the border between Germany and Austria at 2,650 m above sea level (Sigmund et al., 2019), and the Sonnblick Observatory, in the Austrian Alps at an altitude of 3,106 m above sea level (Grasserbauer et al., 1994).

https://doi.org/10.5194/egusphere-2026-1299
Preprint. Discussion started: 13 March 2026

This study presents the first continuous, highly time-resolved measurements of aerosol microphysical and optical properties at high elevation in the southern edge of the western Alps, spanning a 21-month period. Observations were conducted at the Testa Grigia observatory (3480 m a.s.l.), located on the border between Italy and Switzerland (Apadula et al., 2019). We begin by characterizing the aerosol microphysical properties observed at Testa Grigia and their temporal variability. We then apply an unsupervised classification approach and model back trajectory analysis to identify the aerosol populations reaching the observatory and their transport mechanisms. Finally, we investigate episodes of Saharan dust transport, assessing their impact on aerosol microphysical properties and their temporal variability.

2. Materials and Methods

2.1 Testa Grigia Observatory

Aerosol measurements are performed continuously at the Testa Grigia Observatory (45.93436° N, 7.70778° E, 3480 m asl), near Plateau Rosa glacier, in the north-western Italian Alps (Fig. S1a). The observatory hosts the Plateau Rosa monitoring station of greenhouse gases, which is part of the Global Atmospheric Watch (GAW) network and is one of the highest stations in the program (Apadula et al., 2019). Due to its remote and high-altitude location, the observatory is often above the boundary layer and gas and aerosol-phase measuremenrs are representative of background conditions. Local potential contamination sources could affect Testa Grigia during daytime and include snowmobiles for ski-area maintenance and a nearby mountain hut. In addition, during part of the investigated period, construction activities for building of a new cable car station nearby the observatory and involving the employment of diesel-fueled machinery and local soil resuspension must be reported. The construction site was operative between 6:00 and 18:00 during weekdays. Potential contaminated periods were removed from our analysis.

Windrose from 1-minute time resolution data (Fig. S1b) indicates that the prevailing wind directions are from south-west and from north-east, with no specific day/night circulation. Wind speed higher than 8 m/s was recorded for 35% of the measurement period, and 31% of the time the direction was from North to East. No significant differences in wind pattern are observed among seasons. Temperature at Testa Grigia is characterized by a clear seasonality, with higher values in summer (June - August average was equal to 3.3°C ± 3.3°C) and lower in winter (December - February average was equal to -9.8°C ± 5.9°C), while the diurnal temperature range does not show significant seasonal differences, with annual average equals to 6.6°C ± 2.3°C (Fig. S1c).

2.2 Aerosol measurements

The particle number size distribution is measured in the range of 0.25 µm to 35 µm, using an Optical Particle Counter (OPC, model Grimm EDM 264). The OPC operates at a flow rate of 1.2 liters per minute and categorizes individual particles by their optical diameter across 31 channels. This classification is based on the intensity of light scattered by particles when illuminated by a laser diode (Kulkarni et al., 2011). In this study, fine particles are defined as having an optical diameter between 0.3 µm and 1 µm, whereas coarse particles have diameters greater than 1 µm.

The OPC unit is equipped with a cabinet for outdoor installation and is characterized by a µ-Sigma-2 inlet equipped with a 50 cm heated probe that allowed the operation at temperature as low as -20°C and windspeed up to 40 m/s. Relative humidity (RH) is continuously monitored inside the sampling line and measurement corresponding to RH larger than 40% were discarded from analysis (1.8% of datapoints). To exclude potential contamination from local sources, the OPC data at 1-minute time resolution were corrected according to Beck et al. (Beck et al., 2022) using the same parameters applied to particle number size distribution measurements collected at a high elevation site. This criterion identified 13%

https://doi.org/10.5194/egusphere-2026-1299
Preprint. Discussion started: 13 March 2026

of data points as potentially affected by local pollution sources. Hourly concentrations were calculated from 1-minute time resolution data.

Absorption coefficient of total suspended particles is measured at seven wavelengths (370, 470, 520, 590, 660, 880, and 950 nm) since February 2022 by an aethalometer (AE33, Magee Scientific) at 1-minute time resolution using a sampling flow rate of 3 lpm. The aethalometer derives the aerosol absorption coefficient by measuring the increment of light attenuation produced by aerosol deposited continuously onto a filter tape, based on the following equation (Drinovec et al., 2015):

$$B_{abs} = \frac{dATN}{dt} \cdot \frac{S}{F} \cdot \frac{1}{(1 - k \cdot ATN)} \cdot \frac{1}{C} \quad (1)$$

Where dATN is the attenuation increment observed during time interval dt, S is the aerosol deposition area on the filter, and F is the sampling flow rate. The terms 1/C and (1 – k ATN) are introduced in the formula to correct for measurement artifacts related to light multiple scattering and loading effect, respectively. Multiple scattering artifacts depend on the filter tape and on the optical properties of collected aerosol. In this study we used wavelength-dependent C-values derived by Yus-Diez et al. (2021) for filter tape M8060 and for the mountain site. Loading artifacts depend on accumulation of aerosol on the filter (and thus on attenuation ATN) and can lead to an absorption coefficient underestimation due to particles embedded in the filter or hidden by other particles (Weingartner et al. 2003). To correct for this effect, the AE33 collects aerosol particles on two filter spots at different flow rate, and the comparison of the attenuation between the two spots allows the calculation of the correction parameter k (Drinovec et al., 2015).

To reduce noise of absorption coefficient measurements, especially for values close to the detection limit, the absorption coefficient was calculated applying formula (1) over a time increment of 20 minutes. Following, measurements affected by local contamination were identified and removed (Beck et al., 2022). Aerosol absorption coefficients are reported at standard temperature and pressure.

2.3 Meteorological and automated lidar ceilometer measurements

To investigate local and regional circulations, we analyzed wind speed, wind direction, and specific humidity measurements collected at 30-min time resolution at four stations: Maen, Breuil, Cime Bianche (located in the Valtournenche Valley) and Donnas (in the main Aosta Valley). The coordinates and altitudes of these stations are reported in Table S2, while their locations are shown in Fig. S2b. All meteorological data are available on the Aosta Valley regional webpage (Ravda).

Information on the evolution of the aerosol boundary layer over the valley, reflecting the combined influence of turbulent mixing and thermally driven slope and valley winds, was derived from measurements collected by an Automated Lidar Ceilometer (ALC) located at Saint-Christophe (45.75°N, 7.21°E, 560 m a.s.l.), approximately 40 km west of Testa Grigia. The station is equipped with a Lufft CHM15k ALC, a single channel, bistatic instrument operating at 1064 nm that continuously probes aerosol vertical profiles with high vertical (15 m) and temporal (15 s) resolution up to 15 km altitude. To trace the aerosol boundary layer dynamics, we used the height of the Continuous Aerosol Layer (CAL) as a proxy metric. Derived from the ALC profiles, the CAL is defined as the layer extending from the surface marked by a continuous presence of aerosols throughout its depth, above which the atmosphere is predominantly aerosol-free (Bellini et al., 2025). This enables the separation of boundary layer aerosols from free tropospheric conditions.

2.4 Cluster analysis

https://doi.org/10.5194/egusphere-2026-1299
Preprint. Discussion started: 13 March 2026

The average particle volume size distribution is calculated on an hourly basis, assuming that the particles are spherical. For each size bin, the particle volume concentration is determined using the following formula, where Dp is the geometric mean of the upper and lower size limits of each bin:

$$n_V(D_p) = \frac{\pi}{6} n_N(D_p) \quad (2)$$

while total volume concentration is the sum of particle volume concentrations over multiple size bins, as follows:

$$V = \frac{\pi}{6} \sum_{bin=1}^{22} D_{p\,bin}^3 \; n_N(D_{p\,bin}) \quad (3)$$

For cluster analysis, we focused solely on particle numbers measured in the first 22 size bins, which correspond to optical diameters smaller than 9.4 µm. Volume size distribution data were analyzed using k-means cluster analysis. Hourly volume size distributions were first normalized relative to the integrated volume to ensure that the analysis focused solely on the shape of the size distribution curves rather than on the absolute volume concentration. Then, for each size, volumes were standardized (mean equal to zero and standard deviation equal to 1) to give equal importance to all particle size bins. We used Euclidean distance as the measure for clustering (Hartigan-Wong algorithm). The optimal number of clusters was determined by maximizing the similarity among the elements within each cluster while keeping the total number of clusters as low as possible. We used the Silhouette index to measure the similarity and dissimilarity of each object within the same cluster and between different clusters. In contrast, the total within-cluster sum of squares serves as an indicator of the similarity among objects within each group.

2.5 Analysis of synoptic scale transport

Seven-day back trajectories were calculated using LAGRANTO (Sprenger and Wernli, 2015; Wernli, 1997). Trajectory were calculated every 6 hours and initialized at the Testa Grigia exact position and at 4 additional positions around the observatory, corresponding to ± 0.5 degrees latitude and longitude. Per each position, 4 pressure levels were considered: surface pressure and 10 hPa, 30 hPa, and 50 hPa below surface pressure. Input meteorological data for trajectory calculation were ERA5 data with a horizontal resolution of 0.5° × 0.5° and a vertical resolution of 137 levels up to 1 hPa. The duration of seven days was selected in agreement with atmospheric residence time of fine anthropogenic aerosol as well as traveling time of dust particle from north Africa (Collaud Coen et al., 2004). Although the complex alpine terrain orography is poorly resolved in ERA5, the back trajectory analysis still offers a first guidance about the air mass origin. To calculate the time that back trajectories spend over land and water we used a land-sea mask at 0.1° x 0.1° from NASA (Nasa) that was re-sampled at 0.5x0.5 degree resolution to match back trajectory spatial resolution.

Potential Source Contribution Function (PSCF) maps (Ashbaugh et al., 1985) were created for the latitude range of 20° N to 60° N and the longitude range of 20° W to 30° E, with a resolution of 0.5° x 0.5°. These maps were generated by calculating the number of hours (or passes) that back trajectories spent in each grid cell when the total and coarse particle number exceeded the 75th percentile and the trajectory was in the lower troposphere (trajectory pressure within 150 hPa from surface pressure). This value was then divided by the total number of passes per each cell. PSCF values were adjusted using a weight function to minimize the impact of grid cells that had a limited number of passes (Sun et al., 2015).

2.6 CAMS ensemble model

To support the analysis and to complement the in-situ observations at Testa Grigia, surface-level concentrations of PM_{10} and dust were extracted from the CAMS European Air Quality Reanalyses dataset (Cams, 2021). In this dataset, dust

https://doi.org/10.5194/egusphere-2026-1299
Preprint. Discussion started: 13 March 2026

represents the mineral dust fraction of total PM_{10}, provided as a separate model output field. The CAMS reanalysis dataset covers the entire European domain with horizontal resolution of 0.1° × 0.1° and delivers hourly three-dimensional fields of the main atmospheric pollutants. It is generated from an ensemble of eleven regional air-quality modelling systems developed in Europe, all driven by the same operational meteorology from the European Centre for Medium-Range Weather Forecasts (ECMWF). In addition, the individual models within the ensemble apply consistent chemical boundary conditions derived from the global CAMS system, use CAMS-based European emission inventories, and assimilate the same set of surface air-quality observations (MaréCal et al., 2015).

The ensemble median product was selected, given that ensemble statistics generally provide a more accurate representation of pollutant concentrations over Europe than any single model member (Peuch et al., 2022). The high-resolution CAMS ensemble is recognized for its performance and representativeness in long-term aerosol and dust assessments across Europe, as supported by several recent studies (Tositti et al., 2022; Ramesh et al., 2025; Yadav et al., 2025; Bellini et al., 2025).

3. Results

3.1 Microphysical aerosol properties

Figures 1a and 1b present the time series of hourly fine (particles with optical diameter between 0.25 μm and 1 μm) and coarse (particles with optical diameter between 1 μm and 10 μm) particle number, respectively, along with monthly data capture (which represents the number of available hourly data points normalized by the total number of hours in the month). Overall, data capture was generally higher than 60%, except for January (40%) and November 2022 (45%).

During the entire investigation period, the median of the total particle number concentration (PNC) (optical diameter larger than 0.25 μm) was 4.53 particles/cm³, with an interquartile range (IQR) of 1.27-18.34 particles/cm³. The median fine particle number concentration was 4.46 particles/cm³ (IQR 1.24 -18.05 particles/cm³), while the coarse particle number concentration was 0.03 particles/cm³ (IQR 0.01-0.09 particles/cm³). The seasonal statistics of total, fine, and coarse PNC are provided in Table S1. The highest concentration of fine particles was recorded in summer (June-August), while coarse particles peaked in spring (March-May), primarily due to a significant dust event that took place in March 2022, as reported by observations and models (Wmo, 2023; Cuevas-Agulló et al., 2024). This event caused the coarse PNC at Testa Grigia to reach values as high as 83 particles/cm³. Throughout all seasons, fine particles consistently dominated the particle number concentration.

The average concentration of PNC at Testa Grigia and its seasonality (Table S1) are similar to those observed in comparable size ranges at other high-altitude stations. At Monte Cimone (2165 m asl), in the Italian Apennines, the average concentration of fine with an optical diameter between 0.3μm and 1 μm) and coarse particles (with an optical diameter larger than 1 μm) over multiple years were 26.15 ± 37.64 cm^{-3} and 0.17 ± 0.59 cm^{-3}, respectively (Marinoni et al., 2008). Xu et al. (Xu et al., 2013) reported that seasonal average PNC in the range 0.25 μm – 32 μm at Qilian Shan Station (Qinghai-Xizang Plateau, 4180 m asl) varied between 34 ± 41 cm^{-3} in summer and 17 ± 28 cm^{-3} in fall. Nyeki et al. (Nyeki et al., 1998b) investigated PNC at Jungfraujoch (3580 m asl), where the monthly average concentration of coarse particles (with an optical diameter above 1 μm) ranged from 0.01 to 0.14 cm^{-3} in free tropospheric conditions and from 0.01 to 0.24 cm^{-3} in planetary boundary layer conditions.

https://doi.org/10.5194/egusphere-2026-1299
Preprint. Discussion started: 13 March 2026

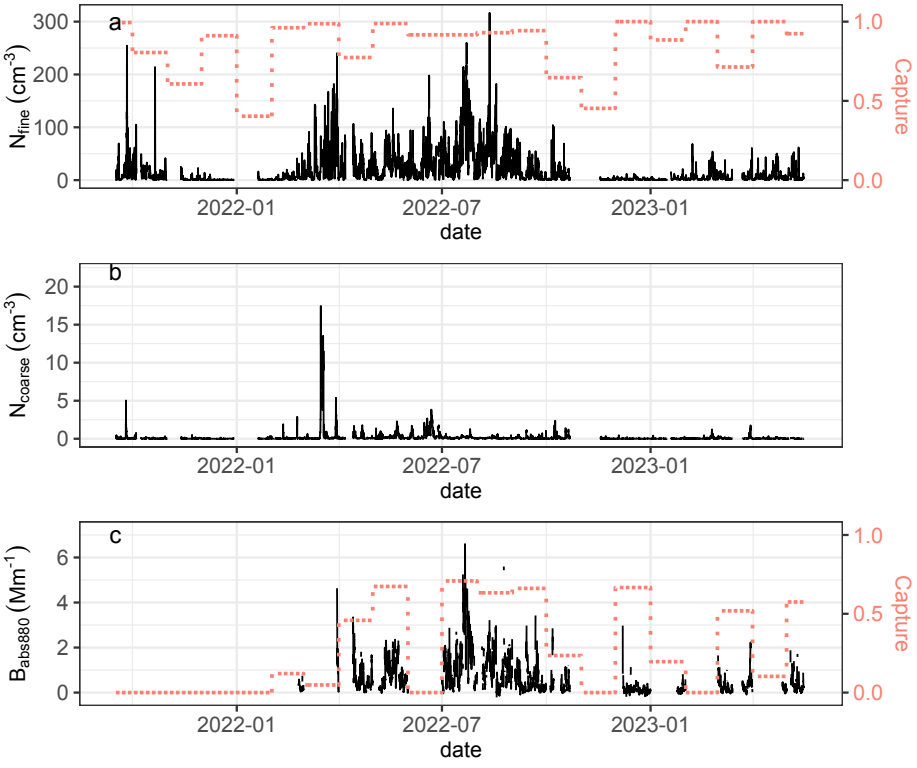

Figure 1. Time series of fine (panel a) and coarse (panel b) hourly PNC together with hourly aerosol absorption coefficient at 880 nm (panel c); right axis of panel a and c report the data capture of PNC and absorption coefficient measurements, respectively.

Aerosol light absorption coefficient measurements began in March 2022 but experienced breaks due to instrumental failure. As data capture exceeded 50% in only a limited number of months, seasonal variability is not discussed. Nevertheless, in the following section, where absorption coefficient measurements overlap with particle number size distribution observations, the absorption data are used to support the discussion of aerosol population types identified solely based on OPC data.

3.2 Classification of aerosol population types

As previously outlined, we analyzed hourly particle volume size distribution using cluster analysis. The optimal classification was achieved by setting the number of clusters to three, a configuration that maximized the average Silhouette index while minimizing the total within-cluster sum of squares. Box-whisker plot in Fig. 2 (panels a to c) reports the variability of particle volume size distribution calculated for the three identified clusters, while Fig. 2d shows their monthly occurrence probability.

https://doi.org/10.5194/egusphere-2026-1299
Preprint. Discussion started: 13 March 2026

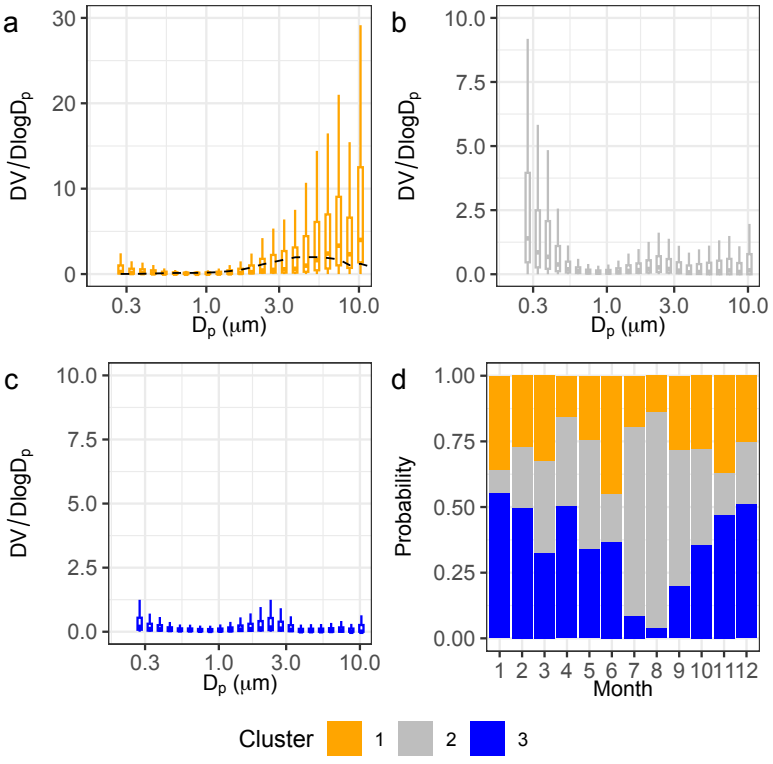

Figure 2. Particle volume size distribution corresponding to the three clusters (a is cluster 1, b is cluster 2, and c is cluster 3): lines indicate 5th-95th percentile ranges, bars correspond to 25th-75th percentile ranges, while markers indicate median values; black dotted line in panel a is the average median size distribution corresponding to the intense dust event of March 2022.

The first cluster is the one characterized by the highest internal similarity (i.e. highest silhouette index, equal to 0.40), and the smaller fraction of datapoints (27%). The size distribution of particle volume concentration of this cluster shows the highest values between 3 and 10 μm. This cluster corresponds to the periods when the largest concentration of coarse mode particles was observed. The average number of coarse particles was 0.4 ± 1.2 particles/cm^3 which is about 6 times higher than the mean values recorded for cluster 2 and 3. This cluster likely corresponds to long-range dust transport events. To support this interpretation, we observed that in spring 2022, an intense Saharan dust transport episode affected Europe, reaching Italy from March 15 to March 18 (Wmo, 2023; DiéMoz et al., 2025). During this event, the coarse particle number concentration at Testa Grigia averaged 7.5 ± 3.6 particles/cm^3, approximately 70 times higher than the campaign average. Concurrently, particle depolarization ratios measured by a polarization-sensitive ALC in Saint-Christophe increased from 5% to 35% in the 2000–4000 m a.s.l. layer, clearly indicating the presence of non-spherical mineral dust particles. The dust intrusion caused the sky to take on shades of orange, which was clearly visible in images captured by the live webcam nearby the observatory. The average particle volume size distribution observed during the March dust event is represented by a black dashed line in Fig 2a and resembles that of cluster 1, with a peak in volume concentration around 3 μm, in agreement with previously reported size distribution of long-range transport of Saharan

https://doi.org/10.5194/egusphere-2026-1299
Preprint. Discussion started: 13 March 2026

dust (Kahn et al., 2009; Schwikowski et al., 1995). This cluster is observed during all seasons, with seasonal average contributions ranging between 24% and 31%. The presence of dust during periods identified by cluster 1 is confirmed by a relatively high values of the average absorption coefficient ($Babs_{880nm}$ = 0.64 ± 0.75 Mm^{-1}) and Absorption Ångström Exponent ($AAE_{370-950}$ = 1.56 ± 0.33).

The second cluster exhibits a relatively high internal silhouette index of 0.39 (high cluster internal similarity) and accounts for 35% of datapoints. Its average volume size distribution is marked by the highest values in the submicron range, with concentrations increasing as the optical diameter decreases. This cluster represents aerosol population whose volume size distribution is dominated by accumulation mode particles rather than coarse mode particles, and the corresponding average fine particle number concentration was 31 ± 38 particles/cm^3. Cluster 2 dominates summer observations (June – August), with a seasonal average contribution equal to 58%. This cluster is associated with the highest average aerosol absorption coefficient ($Babs_{880}$ = 0.98 ± 0.90 Mm^{-1}) and the lowest AAE ($AAE_{370-950}$ = 1.48 ± 0.24), which are indicative of slightly higher absorbing and darker particles. Nevertheless, the limited availability of aerosol optical measurements during the investigated period prevents the analysis of optical properties seasonal variability.

The third cluster is characterized by the highest internal variability, reflected in a low silhouette index of 0.26. This cluster comprises the largest share of data points (37% of the total) and, on average, is characterized by low concentration of both accumulation and coarse mode particles, although a slight increase in particle number concentration is still observed around 3 μm. Cluster 3 is observed mainly in winter months (December – February), with an average share of 52%. The average concentrations of fine and coarse particles number associated with cluster 3 were 5.8 ± 10.4 particles/cm^3 and 0.1 ± 0.1, respectively. Cluster 3 is the one characterized by the lowest average aerosol absorption coefficient ($Babs_{880}$ = 0.35 ± 0.37 Mm^{-1}) indicating negligible impact of light absorbing particles. Based on ALC measurements, 71% of the time when the particle size distribution is classified into cluster 3, the observatory is outside the continuous aerosol layer.

4. Discussion

4.1 Aerosol transport mechanisms

4.1.1 Boundary layer influence

Mountain observatories can be impacted by the vertical transport of aerosols from lower altitudes, which is influenced by the development of the boundary layer and by thermally driven mountain slope winds (Collaud Coen et al., 2018). These thermally driven circulations are particularly effective at transporting air masses from the boundary layer up to high elevations, particularly in spring and summer (Zardi and Whiteman, 2012). On fair weather days, solar radiation heats the surface at sunrise, warming the air in the valley and triggering pressure gradients between the valley and the plain (upvalley flow) and between the valley floor and the surrounding slopes (upslope flow). Conversely, at sunset, the valley and the mountain slopes cool more rapidly than the air over the plain and valley floor, causing downvalley and downslope winds. This type of atmospheric circulation results in a distinct diurnal pattern in the concentration of aerosols, trace gases, and water vapor at mountain observatories, with higher concentrations observed in the late morning and afternoon (Andrews et al., 2011; Baltensperger et al., 1997).

Figure 3 shows the daily cycle of the occurrence frequency of the three clusters for each month. The specific humidity ratio (i.e. the ratio between Testa Grigia and Donnas specific humidity) is also reported as a proxy for the transport of moist, boundary layer air masses to the observatory. During the colder months—January, February, November, and December—when atmospheric stability prevents convective motions in the lower troposphere, Cluster 3 (clean air masses) is the most frequently observed cluster throughout the day. In contrast, during the warmer months (July, August,

https://doi.org/10.5194/egusphere-2026-1299
Preprint. Discussion started: 13 March 2026

and September), Cluster 2 (characterized by an aerosol population dominated by accumulation mode particles) is the most prevalent, due to atmospheric instability favoring vertical mixing, and to mesoscale and long range-transport of polluted air masses. In the remaining months, clean air masses tend to be more frequent in the night and morning hours, while accumulation mode particles are more frequently observed in the afternoon. In particular, in March, April, and June, the diurnal profiles of cluster 2 and 3 frequency mirror each other and cluster 2 becomes prominent when the specific humidity ratio starts to increase, indicating that in the transition season the mountain slope winds have a discriminating role in controlling the timing of accumulation aerosol population transport to high elevations in the Alps.

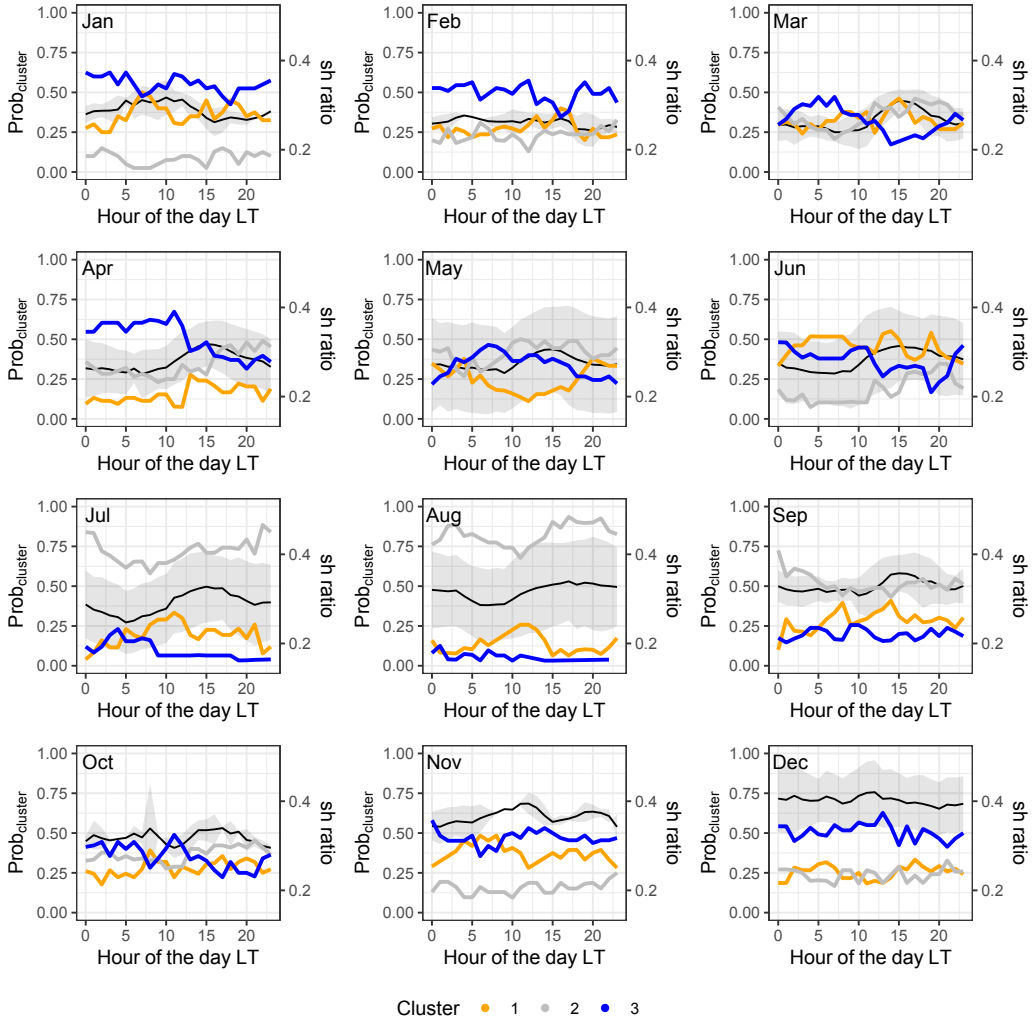

Figure 3. Monthly diurnal variability of cluster occurrence frequency (cluster 1 in orange, cluster 2 in gray, and cluster 3 in blue) together with diurnal variability of the specific humidity ratio (black line corresponds to the average while shaded area is the standard deviation range).

https://doi.org/10.5194/egusphere-2026-1299
Preprint. Discussion started: 13 March 2026

To further assess the influence of boundary layer dynamics on cluster 2, Fig. 4 reports the variability of particle number concentration for the three clusters as a function of the continuous aerosol layer height (calh) measured at Saint Christophe. Panels a-c shows that the aerosol population type corresponding to cluster 2 is the most frequently observed (48% of the time) when the observatory is located within the continuous aerosol layer. In such condition, the particle number concentration of this cluster reaches highest values compared to the other two clusters. Furthermore, during periods of high aerosol anomaly (panels d-f), the average particle number concentration for clusters 1 and 3 remain consistent regardless of the continuous aerosol layer height, while for cluster 2 the number of particles increases on average by 25% when the observatory is within the continuous aerosol layer.

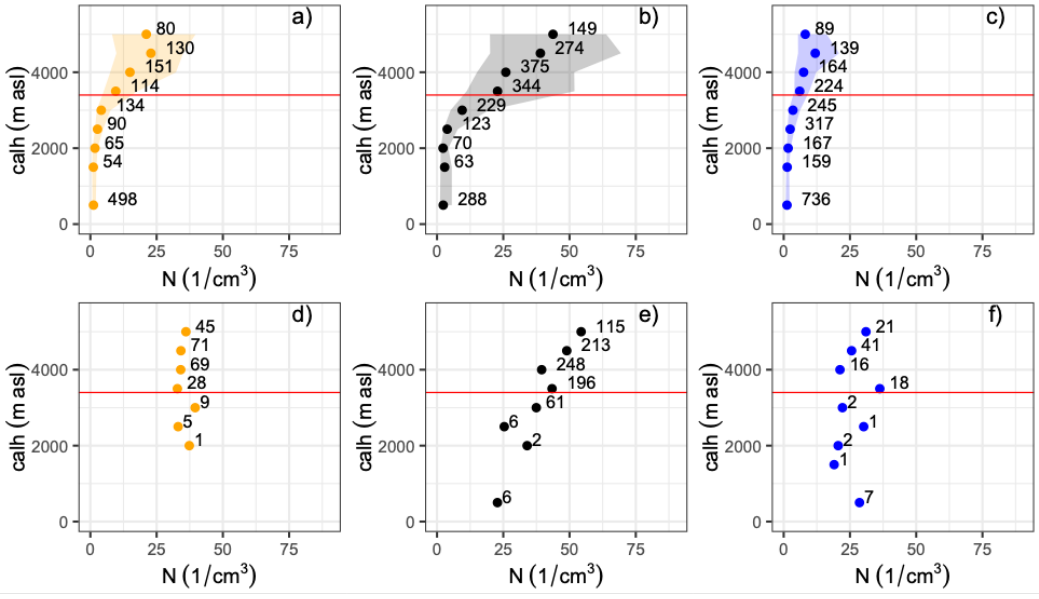

Figure 4. Average particle number concentration as a function of continuous aerosol layer height (calh) for the three different clusters during the entire observation period (panels a – c) and when particle number concentration exceeded the 75th percentile (panels d -f); the shaded areas indicate the 25th-75th percentile range, the number close to each marker indicate the number of observations corresponding to each altitude bin, while the red line indicates the altitude of the Testa Grigia observatory.

These findings collectively suggest that during the warmer months, boundary layer air masses influence the diurnal variability of aerosol particle concentrations and contribute to the enhancement of the accumulation-mode aerosol population at Testa Grigia. If we assume that boundary layer influence corresponds to periods when the observatory was situated within the continuous aerosol layer, and that the associated aerosol population aligns with cluster 2, we can infer that boundary layer air masses impacted the observatory for approximately 28% of the study period. However, this estimate should be regarded as an upper bound, as the contribution from long-range transport has not been excluded. Ongoing analyses using a new 3-d-version of the model employed by Baltensperger et al. (1997) aim to disentangle the respective influences of local and remote aerosol sources.

https://doi.org/10.5194/egusphere-2026-1299
Preprint. Discussion started: 13 March 2026

4.1.2. Regional and synoptic scale transport

The analysis of the air mass history prior to reaching the observatory helped us characterize the effects of regional scale (less than 100 km around Testa Grigia) and synoptic scale (around 1000 km around Testa Grigia) transport on the aerosol population types observed at Testa Grigia. Figure 5 presents the Potential Source Contribution Function (PSCF) maps calculated for the three clusters when aerosol particle concentrations exceeded the 75th percentile, using both 24-hour and 7-day back trajectories. Only trajectory points within a 150 hPa deep layer above the surface were retained for map calculation, to account for the influence of surface processes and emissions (Collaud Coen et al., 2004). The analysis of the 24-hour air mass history (panels a-c) allows us to identify the impact of nearby source areas via regional scale transport, while the longer back trajectories (panels d-f) provide insights into the effects of synoptic scale transport from remote sources.

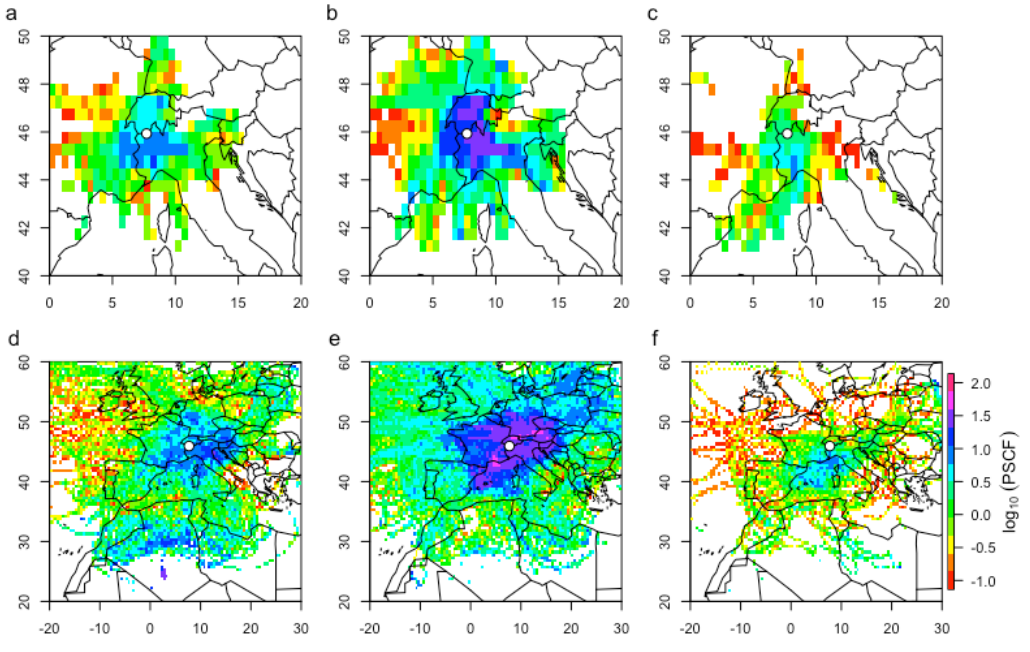

Figure 5. PSCF maps of 24-hours back trajectories (a to c) and 7-days back trajectories (d to f) for cluster 1 (a and d), cluster 2 (b and e), and cluster 3 (c and f), when total particle number concentration was larger than the 75th percentile. The white circle indicates the position of the Testa Grigia observatory.

At the regional scale, the PSCF map for cluster 2 exceeded 25% over the Po Valley and northern Switzerland, indicating that aerosol and aerosol precursors emitted from these regions likely contribute to the population of accumulation mode particles observed at Testa Grigia within a time frame shorter than 24 hours. Clusters 1 and 3, on the other hand, show no specific regional origin in the considered domain, pointing towards the potential impact of long-range transport.

The influence of the Po Plain outflow on the aerosol population, particularly the accumulation mode particles at Testa Grigia, is further supported by the analysis of the prevailing wind patterns in the southern valley. Figure S2 illustrates that higher particle number concentrations in cluster 2 are more frequently observed at Testa Grigia when air masses move from south to north and when the wind direction favors the transport from the Po Plain. Notably, during wind conditions

https://doi.org/10.5194/egusphere-2026-1299
Preprint. Discussion started: 13 March 2026

that favor transport from the Po Plain, the particle number concentration linked to cluster 2 was 60% higher than the campaign average.

At the synoptic scale, the PSCF map of cluster 1 shows relatively higher values over northern Africa, confirming that this cluster is representative of an aerosol population affected by long-range transported dust. Nevertheless, the function values in this region are generally below 10%, likely due to the variability of dust source strength (Knippertz and Todd, 2012). In contrast, the map of cluster 2 indicates the larger PSCF values over northern Italy, central and eastern Europe, highlighting the contribution of European continental emissions to the accumulation mode aerosol population observed in the high-altitude Alps. Finally, the map of cluster 3 shows higher values over the western Mediterranean Sea, indicating transport of marine air masses. The link between cluster 3 aerosol population and air masses less affected by pollution sources is confirmed by the fact that back trajectories associated to this cluster spent 13% of the time over water and 63% in the free troposphere.

To summarize, we observe that emissions from the Po Valley can affect Testa Grigia aerosol population dominated by accumulation mode particles within a time frame of less than 24 hours, while transport from central and eastern Europe can have an impact on longer time scale. Conversely, the occurrence of aerosol population dominated by coarse particles, represented by cluster 1, is primarily driven by the transport of air masses from northern Africa at a synoptic scale.

4.2 Saharan Dust Events (SDE)

The analysis of aerosol microphysical properties and their origin confirms that Testa Grigia is affected by Sharan dust transports. To assess the impact of Saharan dust transport in the high elevation Alps, we first identify Saharan Dust Events (SDE) periods, we then discuss their impact on the aerosol concentration and optical properties, and finally we investigate variability of dust transport events based on synoptic scale dynamics.

Previous works discriminated SDE at mountain sites combining air mass history with aerosol size distribution data (Vogel et al., 2025; Duchi et al., 2016) or aerosol optical properties (Collaud Coen et al., 2004). In this work we identified SDE as those periods when the aerosol size distribution was dominated by coarse particles (i.e. period falls into cluster 1) and air masses passed over the Sahara Desert, at low altitudes (trajectory pressure within 150 hPa from surface pressure), during the 7 days prior the arrival at Testa Grigia. This innovative approach avoids the need for defining an arbitrary concentration threshold for coarse particles, thereby reducing potential subjectivity in SDE identification.

Overall, Testa Grigia experienced Saharan dust transport for 754 hours over 21 months (6% of the measurement time), corresponding to 62 SDE with a duration of at least 4 hours. This number of events is comparable with that reported for Jungfraujoch during a similar time span in the early 2000s' (Collaud Coen et al., 2004). Most of the episodes had a duration shorter than 10 hours, but from March to June we observed a few events lasting from 24 up to 46 hours, in agreement with long time series observations in the Apennines, reporting more frequent multi-day's events in summer (Vogel et al., 2025).

The identification of SDE based on observations was compared with the output of the ensemble CAMS model (Fig. 6). We estimated PM_{10} mass concentration during the SDE from particle size distribution assuming a spherical shape and a size dependent density (Wittmaack, 2002). CAMS reported non-zero dust concentrations for most of the investigated period (97%), therefore CAMS dust events were defined as periods when the ensemble dust concentration (ENS_dust) exceeded the third quartile plus 1.5 times the interquartile range (i.e. 1.20 $\mu g/m^3$). Dust periods coincided in model and observations (orange markers in Fig. 6a) during the most intense events, when PM10 exceeded 10 $\mu g\ m^{-3}$, although CAMS consistently underestimated observed PM_{10} levels by about 33%. In contrast, hourly data points classified as SDE in the observations but associated with lower PM10 were not correctly identified by CAMS (green markers in Fig. 6a), reflecting

https://doi.org/10.5194/egusphere-2026-1299
Preprint. Discussion started: 13 March 2026

the limitations of a threshold-based criterion. Nevertheless, observed SDE datapoints showed PM_{10} values that correlated reasonably with CAMS predictions (r = 0.48). Conversely, approximately 760 hours were classified as dust-affected by CAMS but not recognized as SDE in the observations (black markers in Fig. 6a). In these cases, CAMS overestimated PM_{10}, likely due to the coarse spatial resolution of the model that might include local sources actually not affecting the observatory. In fact, the relatively high PM_1 to PM_{10} ratio (Fig. 6b) indicate that dust, if present, was mixed with other aerosol types, including anthropogenic and secondary sources, and therefore not attributed to SDE by observations.

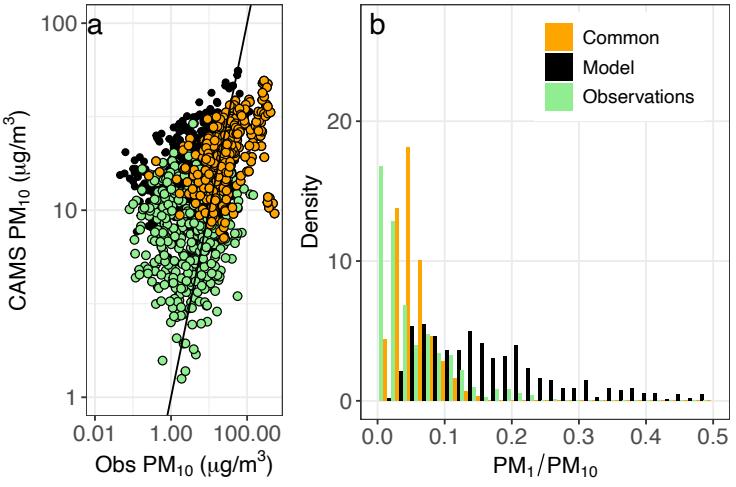

Figure 6. Panel a: comparison between hourly PM10 concentration reconstructed from particle volume size distribution (Obs PM_{10}) and modeled by CAMS (CAMS PM_{10}) (in orange when dust presence is identified by both model and observations, in green when dust is identified exclusively by the observations, and in black when only CAMS detect dust transport); panel b: frequency distribution of the PM_1 to PM_{10} ratio estimated from particle size distribution and corresponding to the types of events.

4.2.1 Aerosol properties during SDE

The median of the hourly PM_{10} concentration during Saharan dust transport was equal to 9.2 µg/m^3 (IQR: 1.9-25.6 µg/m^3). Except for the intense dust episode of March 2022, PM_{10} ranged from less than 1 µg/m^3 up to 80 µg/m^3, in agreement with previous observations in the Alps and in the Apennines (Brunner et al., 2021; Tositti et al., 2013). Between March 15 and March 19 severe dust episode was observed at Testa Grigia and the hourly PM10 concentration reached a peak of 526 µg/m^3, while average PM_{10} concentration over the entire event was equal to 165 µg/m^3. In the same period, similar PM_{10} levels were recorded at Col Margherita (Barbaro et al., 2024), in the eastern Alp, indicating comparable effects of this event on atmospheric composition across the entire Alpine range. At Jungfraujoch, on the northern edge of the alps, the events was observed with the exact same timing, although with lower PM10 values (Nabel), likely due to deposition along transport.

To evaluate the dust impact on daily PM_{10}, we isolate all days when dust transport was observed for at least 4 hours and the resulting dataset, composed by 74 days, was characterized by daily PM_{10} values ranging from 0.2 µg/m^3 to 300 µg/m^3 (on March 16, 2022). 10% of the dust days showed PM_{10} concentration higher than the limit set by the new European air

https://doi.org/10.5194/egusphere-2026-1299
Preprint. Discussion started: 13 March 2026

quality directive of 40 μg/m^3, highlighting the detrimental effect of dust transport on air quality even in high elevation mountain regions.

Data on aerosol optical properties were available for a shorter duration compared to the size distribution dataset analyzed in this study (Fig 1c), and only during 34% of the hours when SDEs were identified. Table 1 presents the corresponding statistics for aerosol absorption coefficients, along with estimates of dust mass absorption coefficients (MAC), derived from the ratio of absorption coefficients to PM_{10} mass. These MAC estimates assume that PM_{10} mass during dust events is predominantly attributable to mineral dust. Statistics for months with greater optical data coverage during SDEs—specifically April, May, July, August, and December, when data availability exceeded 50%—are shown in brackets. These months exhibit mean and median values consistent with those observed across the entire campaign.

	1st quartile	Median	Mean	3rd quartile
Abs_{370} - Mm^{-1}	0.21 (0.13)	0.85 (0.64)	2.83 (2.68)	5.52 (5.17)
Abs_{520} - Mm^{-1}	0.14 (0.08)	0.63 (0.51)	1.52 (1.44)	2.91 (2.83)
Abs_{880} - Mm^{-1}	0.08 (0.06)	0.35 (0.29)	0.72 (0.68)	1.35 (1.35)
MAC_{370} - m^2 g^{-1}	1.14 (0.12)	0.22 (0.22)	0.26 (0.26)	0.32 (0.37)
MAC_{520} - m^2 g^{-1}	0.08 (0.08)	0.13 (0.13)	0.16 (0.17)	0.19 (0.22)
MAC_{880} - m^2 g^{-1}	0.03 (0.03)	0.06 (0.06)	0.08 (0.09)	0.10 (0.12)
$AAE_{370-950}$	1.15 (1.09)	1.41 (1.26)	1.38 (1.33)	1.59 (1.63)
$AAE_{370-590}$	1.14 (1.07)	1.49 (1.32)	1.50 (1.42)	1.95 (1.86)
$AAE_{590-950}$	0.97 (0.91)	1.09 (1.09)	1.10 (1.12)	1.20 (1.21)

Table 1. Statistics of aerosol optical properties during SDE and between brackets the statistics corresponding to months when optical data coverage was larger than 50%.

Mineral dust absorption is primarily driven by the presence of iron-bearing minerals such as hematite and goethite (Alfaro et al., 2004), which absorb light at wavelengths below 600 nm. However, the optical properties of mineral dust aerosol populations are influenced by multiple factors, including particle size, morphology, and the distance from emission sources, due to microphysical transformations during atmospheric transport (Ryder et al., 2013; Patterson, 1981). As dust travels over long distances, it can mix with other light-absorbing particles such as black carbon (BC), altering both the mass absorption cross section and the absorption Ångström exponent (AAE) (Scarnato et al., 2015).

At Testa Grigia, the median MAC values for dust were 0.22, 0.12, and 0.06 m²/g at 370, 520, and 880 nm, respectively. These values exceed the upper bounds reported in previous experimental and modeling studies. For example, aerosols generated from resuspended soil dust from the Sahara, Sahel, and Gobi deserts exhibited MAC values between 0.01 and 0.02 m²/g at 660 nm (Alfaro et al., 2004). Similarly, MAC values for dust samples from northern Sahara and Morocco averaged 0.02 and 0.06 m²/g at 530 nm, respectively (Linke et al., 2006). Radiative transfer model simulations suggest that dust MAC at 520 nm typically ranges from 0.03 to 0.06 m²/g (Samset et al., 2018). The elevated MAC values observed in this study likely result from the mixing of dust with BC-rich air masses during transport.

Further evidence of BC contamination is provided by the AAE values measured during SDEs. The observed mean and median $AAE_{370–950}$ values (1.38 and 1.41) are significantly lower than those reported for resuspended Saharan dust (2.5–3.2) (Caponi et al., 2017) or for transported dust unaffected by BC (≈2) (Denjean et al., 2016) but are consistent with values associated with BC-contaminated dust (1-1.5) (Drinovec et al., 2020). Likely regions contributing to BC

https://doi.org/10.5194/egusphere-2026-1299
Preprint. Discussion started: 13 March 2026

contamination along the dust transport pathway include the northern African coast and continental Europe (Ren et al., 2025). The higher AAE at shorter wavelengths observed during SDEs indicates a steeper absorption spectrum of aerosol in the UV region, in agreement with the dust absorption enhancement below 600 nm.

4.2.2 Variability of dust transport

Figure 7a reports the monthly frequency of SDE hours observed during the investigated period at Testa Grigia, together with the monthly PM_{10} medians derived from particle number concentration. The frequency of SDE hours varied between 1% and 18%. The largest frequency of SDE were observed from March to June and in October and November. Although the time frame investigated in this study is quite limited, the observed seasonality agrees with multi-year observations at Jungfraujoch, located at similar altitude in the Swiss Alps (Collaud Coen et al., 2025). In March, May and June, when SDE hourly frequency varied between 7% and 18%, the medians PM_{10} were about 20 μg m^{-3}, while in October and November, although dust transport frequency was larger than 8%, PM_{10} concentration was 2 to 3 times lower, indicating that spring and summer events were associated to a larger transport of aerosol mass.

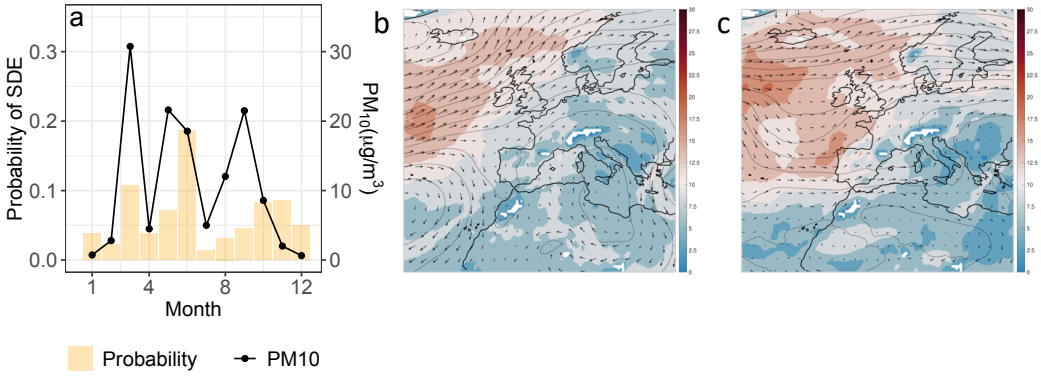

Figure 7. Monthly probability of SDE observed at Testa Grigia, together with the monthly medians of PM_{10} concentration (panel a); maps of average geopotential heights (contour lines; every 20 dam), wind speeds (color; in m/s) and averaged wind arrows over Europe and north Africa during SDE periods in March, May, and June (panel b) and in October and November (panel c).

Saharan dust emissions rate and source spatial distribution vary significantly with season. Saharan dust emissions peaks between February and July, when emission rates are about two times higher compared to the rest of the year (Laurent et al., 2008; Song et al., 2021). Winter and fall dust emissions are limited to Chad, Niger, Mali, and Mauritania, while summer source area extends to the north-western Sahara, leading to significant dust optical depth also over Libya and Algeria (Prospero et al., 2002; Ginoux et al., 2012; Gherboudj et al., 2017).

To explain the transport of dust and the observed variability of PM_{10} mass concentration, fig. 7b and 7c report the maps of the geopotential height and wind speed at 850 hPa during dust events at Testa Grigia in March-May-June and October-November time frames, respectively. The spring and summer events are characterized by the presence of a high-pressure system over the central Mediterranean Sea and Libya and strong northerly winds over Chad, Niger, and Algeria, which favors the transport of dust from the Sahara regions characterized by the highest dust emissions. In fall, dust events are associated with a high-pressure system that extends from Libya further west over Algeria, resulting in intense wind

https://doi.org/10.5194/egusphere-2026-1299
Preprint. Discussion started: 13 March 2026

circulation limited to the regions of the Atlas Mountains over northern Morocco and the coasts of Algeria. In this area and during colder months, dust emissions are lower and controlled by land-use activities (Ginoux et al., 2012). Supplementary Fig S3 reports the maps of back trajectory frequency distribution over the Sahara region during the two considered periods in agreement with the results of the average circulation system here described.

Previous research on Saharan dust export to the Mediterranean, spanning ten to over seventy years, has characterized the associated synoptic-scale dynamics (Pey et al., 2013; Salvador et al., 2014; Salvador et al., 2022). Our findings show that the two circulation systems dominating SDE at Testa Grigia during spring/summer and fall closely resemble the circulation types identified by Salvador et al. (2014; 2022) as driving the largest fraction of dust transport events toward the Iberian Peninsula. This similarity strongly suggests that comparable atmospheric dynamics control the transport of Saharan dust toward both the high-altitude Western and Central Mediterranean. Furthermore, Salvador et al. (2022) reported a significant increase in the occurrence frequency of these circulation types associated with dust outbreaks over the 1948–2020 period (0.77 days per year). Critically, the specific circulation type corresponding to the spring/summer geopotential height maps at Testa Grigia (Fig. 7b) exhibits the largest increasing trend in time, particularly in summer (1.04 days per year).

Another factor that can explain the temporal changes of dust PM_{10} at Testa Grigia is the variability of dust transport efficiency. Particles that move in the middle and upper troposphere are transported more efficiently and over longer distances because they are less affected by removal through cloud scavenging and gravitational deposition. The maps depicting geopotential heights and wind speeds at different pressure levels (500 hPa, 700 hPa, and 850 hPa, Fig. S4), along with dust concentration maps (Fig. S5), indicate that during the warmer months (March, May, and June) the SDE are linked to a significant geopotential trough over the eastern Atlantic. This trough extends up to 500 hPa (corresponding to an altitude of about 5 kilometers a.s.l.), enabling dust plumes to ascend to high elevations over northern Africa and western Europe. In contrast, in October and November, dust plumes are observed only up to 700 hPa and are characterized by lower concentrations. These findings align with the satellite retrieval analysis of dust spatial distribution, which shows that in the Mediterranean region, the concentration of dust decreases with altitude above 2 kilometers, following this seasonal order: summer (June to August), spring (March to May), fall (September to November), and winter (December to February) (Song et al., 2021). Hence, in addition to the geographical variability of dust source regions and dust mobilization over the source region, the higher dust PM_{10} concentration observed at Testa Grigia in spring and early summer are due to more effective transport pathways.

5. Conclusions

This paper presents the first continuous high resolution measurements of aerosol optical and microphysical properties at a high elevation observatory in the southern slope of the European alpine range. Aerosol particle number and size distribution are consistent with values previously reported in the Alps and in the northern Apennines, and indicate that particles smaller than 300 nm, which dominate total particle number, are more efficiently transported to higher elevations during the warmer season. The median of fine particle number concentration in summer (30.7 particles/cm^{-3}) was about 20 times larger than the winter median (1.3 cm^{-3}). On the contrary, the largest coarse particle number concentration was observed in summer (seasonal median equal to 0.1 μg m^{-3}).

The aerosol population types reaching the observatory were identified using cluster analysis relying on the normalized particle volume size distribution. This choice ensured the classification was independent of the absolute particle concentration. Three aerosol populations were identified. The first aerosol cluster was observed when coarse particle

https://doi.org/10.5194/egusphere-2026-1299
Preprint. Discussion started: 13 March 2026

concentration was higher (0.4 ± 1.2 cm³ on average) and was mainly observed during periods influenced by air masses from long-range transport. On the contrary, the second aerosol cluster corresponded to a population dominated by fine particles (31 ± 38 cm^{-3} on average) and was linked to transport of boundary layer aerosols by mesoscale winds and large scale transport from continental Europe. Finally, the third observed aerosol cluster emerged when the particle number was generally low. This finding agrees with back trajectory analysis, which showed the influence of relatively clean air masses traveling in the free troposphere and passing over the Mediterranean Sea.

The unsupervised classification of aerosol population and model back trajectories enabled us to identify SDEs as those time periods characterized by a larger contribution of coarse particles (type 1) and linked to synoptic transport from the Sahara region. This approach, although similar to those adopted by previous studies, does not rely on the definition of a threshold, thereby mitigating the potential for subjective or arbitrary criteria. This mean that even a limited number of events would be recognized as SDE because the associated aerosol size distribution would significantly be different from the rest of the database, even if such events would not be able to impact the site statistics. Overall, during the investigated period, Testa Grigia experienced 62 SDE with a duration of at least 4 hours. The good correlation between PM10 concentration derived from particle number size distribution and from CAMS ensemble model during these events demonstrate the representativeness of the Testa Grigia observatory to investigate long range dust transport events and the potential for model validation.

Aerosol absorption coefficient measurements, available for only part of the observational period, clearly indicate that the dust reaching the observatory is mixed with black carbon. Given that significant BC emission fluxes originate from both the northern coast of Africa and continental Europe, this critical dust-BC mixing can occur either proximal to the dust emission areas or closer to the receptor site. The effect of this mixing is a significant enhancement of the dust's light absorption capacity, which has profound implications for snow melting in mountain areas (Di Mauro et al., 2019). In fact, the deposition of mineral dust on snow already triggers the snow albedo feedback by inducing surface darkening (Skiles et al., 2018); this surface radiative forcing is fundamental in determining the timing and total amount of meltwater available for ecosystems and society. Enhanced light absorption resulting from the black carbon mixture significantly accelerates the contribution of dust to snowmelt. This finding is particularly salient within the context of climate change, where reduced solid winter precipitation heightens the risk of summer drought, making the accelerated release of meltwater a crucial variable for water resource management.

Despite the relatively limited duration of our 21-month measurement record, the synoptic-scale circulation characterizing SDE at Testa Grigia aligns with patterns reported for dust outbreaks across the Western Mediterranean. These established circulation patterns have shown an increasing frequency of occurrence over the last 70 years. Conversely, no statistically significant trend has been detected in long-term (10- to 20-year) in-situ measurements of dust outbreaks at mountain observatories in the Alps and the Apennines (Vogel et al., 2025; Collaud Coen et al., 2025; Petroselli et al., 2024). This discrepancy might be driven by the substantial interannual variability of dust concentration, which complicates the robust detection of trends over decadal timescales (Collaud Coen et al., 2025). Ultimately, this difference underscores the need for an integrated approach—combining *in-situ* observations, transport modeling, and meteorological re-analysis products—to accurately predict how changes in atmospheric circulation driven by climate change are going to impact regional air quality and climate.

In summary, the dataset here presented from Testa Grigia establishes this high-altitude site as a critical new sentinel for monitoring large scale atmospheric composition and transport dynamics in the European Alps. Our findings not only affirm the consistency of observed aerosol microphysics with long-term observations from high-altitude observatories in

https://doi.org/10.5194/egusphere-2026-1299
Preprint. Discussion started: 13 March 2026

Europe but also underscore the urgent need for an integrated monitoring and modeling strategy to accurately predict and mitigate the evolving impact of long-range dust transport on European climate, air quality, and alpine snow.

Competing interest

At least one of the authors is a member of the editorial board of *Atmospheric Chemistry and Physics*. The authors also have no other competing interests to declare.

Financial support

This project was supported by the Italian Ministry of University and Research (MUR) under the FOE project "Capitale naturale e risorse per il futuro dell'Italia", and by the "LAPSE" project (202283CF7W_PE10_PRIN2022), funded by MUR in the "PRIN22" program.

Author contribution

SG and PB designed the measurement set-up, SG EM MP collected field data, SG analyzed the aerosol property data, AB and HD collected and analyzed meteorological data, CG and MS analyzed CAMS model data, MS performed transport model simulations, SG prepared the manuscript, all the authors revised the manuscript.

Acknowledgements

The authors acknowledge the Department of Earth Systems Science and Environmental Technologies of the National Research Council of Italy for the support in the technical and operational management of the observatory.

References

Alfaro, S. C., Lafon, S., Rajot, J. L., Formenti, P., Gaudichet, A., and Maille, M.: Iron oxides and light absorption by pure desert dust: An experimental study, Journal of Geophysical Research: Atmospheres, 109, 2004.

Andrews, E., Ogren, J. A., Bonasoni, P., Marinoni, A., Cuevas, E., Rodríguez, S., Sun, J. Y., Jaffe, D. A., Fischer, E. V., and Baltensperger, U.: Climatology of aerosol radiative properties in the free troposphere, Atmospheric Research, 102, 365-393, 2011.

Apadula, F., Cassardo, C., Ferrarese, S., Heltai, D., and Lanza, A.: Thirty Years of Atmospheric CO2 Observations at the Plateau Rosa Station, Italy, 10.3390/atmos10070418, 2019.

Ashbaugh, L. L., Malm, W. C., and Sadeh, W. Z.: A residence time probability analysis of sulfur concentrations at Grand Canyon National Park., Atmospheric Environment, 19, 1263-1270, 10.1016/0004-6981(85)90256-2, 1985.

Baltensperger, U., Gäggeler, H. W., Jost, D. T., Lugauer, M., Schwikowski, M., Weingartner, E., and Seibert, P.: Aerosol climatology at the high-alpine site Jungfraujoch, Switzerland, Journal of Geophysical Research: Atmospheres, 102, 19707-19715, 1997.

Barbaro, E., Feltracco, M., De Blasi, F., Turetta, C., Radaelli, M., Cairns, W., Cozzi, G., Mazzi, G., Casula, M., Gabrieli, J., Barbante, C., and Gambaro, A.: Chemical characterization of atmospheric aerosols at a high-altitude mountain site: a study of source apportionment, Atmos. Chem. Phys., 24, 2821-2835, 10.5194/acp-24-2821-2024, 2024.

Beck, I., Angot, H., Baccarini, A., Dada, L., Quéléver, L., Jokinen, T., Laurila, T., Lampimäki, M., Bukowiecki, N., Boyer, M., Gong, X., Gysel-Beer, M., Petäjä, T., Wang, J., and Schmale, J.: Automated identification of local contamination in remote atmospheric composition time series, Atmos. Meas. Tech., 15, 4195-4224, 10.5194/amt-15-4195-2022, 2022.

https://doi.org/10.5194/egusphere-2026-1299
Preprint. Discussion started: 13 March 2026

Bellini, A., Diémoz, H., Gobbi, G. P., Di Liberto, L., Bracci, A., and Barnaba, F.: Aerosols in the Mixed Layer and Mid-Troposphere from Long-Term Data of the Italian Automated Lidar-Ceilometer Network (ALICENET) and Comparison with the ERA5 and CAMS Models, Remote Sensing, 17, 372, 2025.

Brunner, C., Brem, B. T., Collaud Coen, M., Conen, F., Hervo, M., Henne, S., Steinbacher, M., Gysel-Beer, M., and Kanji, Z. A.: The contribution of Saharan dust to the ice-nucleating particle concentrations at the High Altitude Station Jungfraujoch (3580 m asl), Switzerland, Atmospheric Chemistry and Physics, 21, 18029-18053, 2021.

Burrows, S. M., McCluskey, C. S., Cornwell, G., Steinke, I., Zhang, K., Zhao, B., Zawadowicz, M., Raman, A., Kulkarni, G., and China, S.: Ice-nucleating particles that impact clouds and climate: Observational and modeling research needs, Reviews of Geophysics, 60, e2021RG000745, 2022.

CAMS European air quality reanalyses. Copernicus Atmosphere Monitoring Service (CAMS) Atmosphere Data Store, last access: 30 November.

Caponi, L., Formenti, P., Massabó, D., Di Biagio, C., Cazaunau, M., Pangui, E., Chevaillier, S., Landrot, G., Andreae, M. O., and Kandler, K.: Spectral-and size-resolved mass absorption efficiency of mineral dust aerosols in the shortwave spectrum: a simulation chamber study, Atmospheric Chemistry and Physics, 17, 7175-7191, 2017.

Chen, D., Rojas, M., Samset, B. H., Cobb, K., Diongue Niang, A., Edwards, P., Emori, S., Faria, S. H., Hawkins, E., Hope, P., Huybrechts, P., Meinshausen, M., M ustafa, S. K., Plattner, G.-K., and Tréguier, A.-M.: Framing, Context, and Methods. In Climate Change 2021: The Physical Science Basis. Contribution of Working Group I to the Sixth Assessment Report of the IPCC, 2021.

Collaud Coen, M., Andrews, E., Alastuey, A., Arsov, T. P., Backman, J., Brem, B. T., Bukowiecki, N., Couret, C., Eleftheriadis, K., and Flentje, H.: Multidecadal trend analysis of in situ aerosol radiative properties around the world, Atmospheric Chemistry and Physics, 20, 8867-8908, 2020.

Collaud Coen, M., Weingartner, E., Schaub, D., Hueglin, C., Corrigan, C., Henning, S., Schwikowski, M., and Baltensperger, U.: Saharan dust events at the Jungfraujoch: detection by wavelength dependence of the single scattering albedo and first climatology analysis, Atmos. Chem. Phys., 4, 2465-2480, 10.5194/acp-4-2465-2004, 2004.

Collaud Coen, M., Brem, B. T., Gysel-Beer, M., Modini, R., Henne, S., Steinbacher, M., Putero, D., Gini, M. I., and Eleftheriadis, K.: Detection and climatology of Saharan dust frequency and mass at the Jungfraujoch (3580 m asl, Switzerland), EGUsphere, 2025, 1-35, 2025.

Collaud Coen, M., Andrews, E., Aliaga, D., Andrade, M., Angelov, H., Bukowiecki, N., Ealo, M., Fialho, P., Flentje, H., and Hallar, A.: Identification of topographic features influencing aerosol observations at high altitude stations, Atmospheric Chemistry and Physics, 18, 12289-12313, 2018.

Collaud Coen, M., Andrews, E., Asmi, A., Baltensperger, U., Bukowiecki, N., Day, D., Fiebig, M., Fjaeraa, A., Flentje, H., Hyvarinen, A., Jefferson, A., Jennings, S., Kouvarakis, G., Lihavainen, H., Myhre, C., Malm, W., Mihapopoulos, N., Molenar, J., O'Dowd, C., ..., and Laj, P.: Aerosol decadal trends - Part 1: In-situ optical measurements at GAW and IMPROVE stations, Atmospheric Chemistry and Physics, 13, 869-894, 10.5194/acp-13-869-2013, 2013.

Cuevas-Agulló, E., Barriopedro, D., García, R. D., Alonso-Pérez, S., González-Alemán, J. J., Werner, E., Suárez, D., Bustos, J. J., García-Castrillo, G., García, O., Barreto, Á., and Basart, S.: Sharp increase in Saharan dust intrusions over the western Euro-Mediterranean in February–March 2020–2022 and associated atmospheric circulation, Atmos. Chem. Phys., 24, 4083-4104, 10.5194/acp-24-4083-2024, 2024.

Denjean, C., Cassola, F., Mazzino, A., Triquet, S., Chevaillier, S., Grand, N., Bourrianne, T., Momboisse, G., Sellegri, K., and Schwarzenbock, A.: Size distribution and optical properties of mineral dust aerosols transported in the western Mediterranean, Atmospheric Chemistry and Physics, 16, 1081-1104, 2016.

https://doi.org/10.5194/egusphere-2026-1299
Preprint. Discussion started: 13 March 2026

Di Mauro, B., Garzonio, R., Rossini, M., Filippa, G., Pogliotti, P., Galvagno, M., Morra di Cella, U., Migliavacca, M., Baccolo, G., Clemenza, M., Delmonte, B., Maggi, V., Dumont, M., Tuzet, F., Lafaysse, M., Morin, S., Cremonese, E., and Colombo, R.: Saharan dust events in the European Alps: role in snowmelt and geochemical characterization, The Cryosphere, 13, 1147-1165, 10.5194/tc-13-1147-2019, 2019.

Diémoz, H., Barnaba, F., Ferrero, L., Tombolato, I. K. F., Mapelli, C., Bellini, A., Desandré, C., Magri, T., and Zublena, M.: From real-time to long-term source apportionment of PM10 using high-time-resolution measurements of aerosol physical properties: Methodology and example application at an urban background site (Aosta, Italy), EGUsphere, 2025, 1-61, 10.5194/egusphere-2025-5044, 2025.

Drinovec, L., Sciare, J., Stavroulas, I., Bezantakos, S., Pikridas, M., Unga, F., Savvides, C., Višić, B., Remškar, M., and Močnik, G.: A new optical-based technique for real-time measurements of mineral dust concentration in PM 10 using a virtual impactor, Atmospheric Measurement Techniques, 13, 3799-3813, 2020.

Drinovec, L., Močnik, G., Zotter, P., Prévôt, A. S. H., Ruckstuhl, C., Coz, E., Rupakheti, M., Sciare, J., Müller, T., Wiedensohler, A., and Hansen, A. D. A.: The "dual-spot" Aethalometer: an improved measurement of aerosol black carbon with real-time loading compensation, Atmos. Meas. Tech., 8, 1965-1979, 10.5194/amt-8-1965-2015, 2015.

Duchi, R., Cristofanelli, P., Landi, T., Arduini, J., Bonafe', U., Bourcier, L., Busetto, M., Calzolari, F., Marinoni, A., Putero, D., and Bonasoni, P.: Long-term (2002-2012) investigation of Saharan dust transport events at Mt. Cimone GAW global station, Italy (2165 m a.s.l.), Elementa-Science of the Anthropocene, 4, 1-14, 10.12952/journal.elementa.000085, 2016.

Dzepina, K., Mazzoleni, C., Fialho, P., China, S., Zhang, B., Owen, R. C., Helmig, D., Hueber, J., Kumar, S., and Perlinger, J. A.: Molecular characterization of free tropospheric aerosol collected at the Pico Mountain Observatory: a case study with a long-range transported biomass burning plume, Atmospheric Chemistry and Physics, 15, 5047-5068, 2015.

Flato, G., Marotzke, J., Abiodun, B., Braconnot, P., Chou, S. C., Collins, W., Cox, P., Driouech, F., Emori, S., and Eyring, V.: Evaluation of climate models, in: Climate change 2013: the physical science basis. Contribution of Working Group I to the Fifth Assessment Report of the Intergovernmental Panel on Climate Change, Cambridge University Press, 741-866, 2014.

Fyfe, J. C., Kharin, V. V., Santer, B. D., Cole, J. N. S., and Gillett, N. P.: Significant impact of forcing uncertainty in a large ensemble of climate model simulations, Proceedings of the National Academy of Sciences, 118, e2016549118, 2021.

Gallagher, J. P., McKendry, I. G., Macdonald, A. M., and Leaitch, W. R.: Seasonal and diurnal variations in aerosol concentration on Whistler Mountain: Boundary layer influence and synoptic-scale controls, Journal of applied meteorology and climatology, 50, 2210-2222, 2011.

Gherboudj, I., Beegum, S. N., and Ghedira, H.: Identifying natural dust source regions over the Middle-East and North-Africa: Estimation of dust emission potential, Earth-science reviews, 165, 342-355, 2017.

Gilardoni, S., Vignati, E., and Wilson, J.: Using measurements for evaluation of black carbon modeling, Atmospheric Chemistry and Physics, 11, 439-455, 10.5194/acp-11-439-2011, 2011.

Ginoux, P., Prospero, J., Gill, T., Hsu, N., and Zhao, M.: Global-scale attribution of anthropogenic and dust sources and their emission rates based on MODIS deep blue aerosol products, Reviews of Geophysics, 50, 10.1029/2012rg000388, 2012.

Grasserbauer, M., Paleczek, S., Rendl, J., Kasper, A., and Puxbaum, H.: Inorganic constituents in aerosols, cloud water and precipitation collected at the high alpine measurement station Sonnblick: Sampling, analysis and exemplary results, Fresenius' journal of analytical chemistry, 350, 431-439, 1994.

https://doi.org/10.5194/egusphere-2026-1299
Preprint. Discussion started: 13 March 2026

Houghton, J. T., Ding, Y., Griggs, D. J., Noguer, M., Linden, J. v. d., Dai, X., Maskell, K., and Johnson, C. A.: Climate Change 2001: The Scientific Basis. Contribution of Working Group I to the Third Assessment Report of the Intergovernmental Panel on Climate Change, 2001.

Igel, A. L., Ekman, A. M. L., Leck, C., Tjernström, M., Savre, J., and Sedlar, J.: The free troposphere as a potential source of arctic boundary layer aerosol particles, Geophysical Research Letters, 44, 7053-7060, 2017.

Kahn, R., Petzold, A., Wendisch, M., Bierwirth, E., Dinter, T., Esselborn, M., Fiebig, M., Heese, B., Knippertz, P., and Müller, D.: Desert dust aerosol air mass mapping in the western Sahara, using particle properties derived from space-based multi-angle imaging, Tellus B: Chemical and Physical Meteorology, 61, 239-251, 2009.

Kanji, Z. A., Ladino, L. A., Wex, H., Boose, Y., Burkert-Kohn, M., Cziczo, D. J., and Krämer, M.: Overview of ice nucleating particles, Meteorological monographs, 58, 1-1, 2017.

Knippertz, P. and Todd, M. C.: Mineral dust aerosols over the Sahara: Meteorological controls on emission and transport and implications for modeling, Reviews of Geophysics, 50, 2012.

Kulkarni, P., Baron, P. A., and Willeke, K.: Aerosol measurement: principles, techniques, and applications, John Wiley & Sons2011.

Laing, J. R., Jaffe, D. A., and Hee, J. R.: Physical and optical properties of aged biomass burning aerosol from wildfires in Siberia and the Western USA at the Mt. Bachelor Observatory, Atmos. Chem. Phys., 16, 15185-15197, 10.5194/acp-16-15185-2016, 2016.

Laj, P., Klausen, J., Bilde, M., Plass-Duelmer, C., Pappalardo, G., Clerbaux, C., Baltensperger, U., Hjorth, J., Simpson, D., Reimann, S., Coheur, P., Richter, A., De Maziere, M., Rudich, Y., McFiggans, G., Torseth, K., Wiedensohler, A., Morin, S., Schulz, M., ..., and Zardini, A.: Measuring atmospheric composition change, Atmospheric Environment, 43, 5351-5414, 10.1016/j.atmosenv.2009.08.020, 2009.

Laurent, B., Marticorena, B., Bergametti, G., Léon, J. F., and Mahowald, N. M.: Modeling mineral dust emissions from the Sahara desert using new surface properties and soil database, Journal of Geophysical Research: Atmospheres, 113, 2008.

Linke, C., Möhler, O., Veres, A., Mohácsi, Á., Bozóki, Z., Szabó, G., and Schnaiter, M.: Optical properties and mineralogical composition of different Saharan mineral dust samples: a laboratory study, Atmospheric Chemistry and Physics, 6, 3315-3323, 2006.

Marinoni, A., Cristofanelli, P., Calzolari, F., Roccato, F., Bonafè, U., and Bonasoni, P.: Continuous measurements of aerosol physical parameters at the Mt. Cimone GAW Station (2165 m asl, Italy), Science of The Total Environment, 391, 241-251, https://doi.org/10.1016/j.scitotenv.2007.10.004, 2008.

Marécal, V., Peuch, V. H., Andersson, C., Andersson, S., Arteta, J., Beekmann, M., Benedictow, A., Bergström, R., Bessagnet, B., and Cansado, A.: A regional air quality forecasting system over Europe: the MACC-II daily ensemble production, Geoscientific Model Development, 8, 2777-2813, 2015.

Masoom, A., Kazadzis, S., Modini, R. L., Gysel-Beer, M., Gröbner, J., Coen, M. C., Navas-Guzman, F., Kouremeti, N., Brem, B. T., and Nowak, N. K.: Long range transport of Canadian Wildfire smoke to Europe in Fall 2023: aerosol properties and spectral features of smoke particles, EGUsphere, 2025, 1-43, 2025.

National Air Pollution Monitoring Network: https://bafu.meteotest.ch/nabel/index.php/abfrage/start/english, last access: December 2025.

IMERG Land-Sea Mask NetCDF: https://gpm.nasa.gov/data/directory/imerg-land-sea-mask-netcdf, last access: April 2025.

https://doi.org/10.5194/egusphere-2026-1299
Preprint. Discussion started: 13 March 2026

Nicolás, J. F., Castañer, R., Crespo, J., Yubero, E., Galindo, N., and Pastor, C.: Seasonal variability of aerosol absorption parameters at a remote site with high mineral dust loads, Atmospheric Research, 210, 100-109, 2018.

Nyeki, S., Baltensperger, U., Colbeck, I., Jost, D. T., Weingartner, E., and Gäggeler, H. W.: The Jungfraujoch high-alpine research station (3454 m) as a background clean continental site for the measurement of aerosol parameters, Journal of Geophysical Research: Atmospheres, 103, 6097-6107, 1998a.

Nyeki, S., Li, F., Weingartner, E., Streit, N., Colbeck, I., Gäggeler, H. W., and Baltensperger, U.: The background aerosol size distribution in the free troposphere: An analysis of the annual cycle at a high-alpine site, Journal of Geophysical Research: Atmospheres, 103, 31749-31761, 1998b.

Patterson, E. M.: Optical properties of the crustal aerosol: Relation to chemical and physical characteristics, Journal of Geophysical Research: Oceans, 86, 3236-3246, 1981.

Petroselli, C., Crocchianti, S., Vecchiocattivi, M., Moroni, B., Selvaggi, R., Castellini, S., Corbucci, I., Bruschi, F., Marchetti, E., and Galletti, M.: Decadal trends (2009-2018) in Saharan dust transport at Mt. Martano EMEP station, Italy, Atmospheric Research, 304, 107364, 2024.

Peuch, V.-H., Engelen, R., Rixen, M., Dee, D., Flemming, J., Suttie, M., Ades, M., Agustí-Panareda, A., Ananasso, C., and Andersson, E.: The copernicus atmosphere monitoring service: From research to operations, Bulletin of the American Meteorological Society, 103, E2650-E2668, 2022.

Pey, J., Querol, X., Alastuey, A., Forastiere, F., and Stafoggia, M.: African dust outbreaks over the Mediterranean Basin during 2001–2011: PM₁₀ concentrations, phenomenology and trends, and its relation with synoptic and mesoscale meteorology, Atmos. Chem. Phys., 13, 1395-1410, 10.5194/acp-13-1395-2013, 2013.

Prospero, J. M., Ginoux, P., Torres, O., Nicholson, S. E., and Gill, T. E.: Environmental characterization of global sources of atmospheric soil dust identified with the NIMBUS 7 Total Ozone Mapping Spectrometer (TOMS) absorbing aerosol product., Reviews of Geophysics, 40, 2-1-2-31, https://doi.org/10.1029/2000RG000095, 2002.

Pörtner, H.-O., Roberts, D. C., Masson-Demotte, V., Zhai, P., Tignor, M., Poloczanska, E., Mintenbeck, K., Nicolai, M., Okem, A., Petzold, J., Rama, B., and Weyer, N.: IPCC 2019: Special Report on the Ocean and Cryosphere in a Changing Climate, 2019.

Ramanathan, V. and Carmichael, G.: Global and regional climate changes due to black carbon, Nature Geoscience, 1, 221-227, 10.1038/ngeo156, 2008.

Ramesh, J. B., Neophytides, S. P., Livadiotis, O., Hadjimitsis, D. G., Michaelides, S., and Anastasiadou, M. N.: Reliability Evaluation of CAMS Air Quality Products in the Context of Different Land Uses: The Example of Cyprus, Environmental and Earth Sciences Proceedings, 35, 64, 2025.

RAVDA, C. F.: Database Centro Funzionale Regione Autonoma Valle d'Aosta [dataset],

Regayre, L. A., Johnson, J. S., Yoshioka, M., Pringle, K. J., Sexton, D. M. H., Booth, B. B. B., Lee, L. A., Bellouin, N., and Carslaw, K. S.: Aerosol and physical atmosphere model parameters are both important sources of uncertainty in aerosol ERF, Atmospheric Chemistry and Physics, 18, 9975-10006, 2018.

Ren, Y., Oxford, C. R., Zhang, D., Liu, X., Zhu, H., Dillner, A. M., White, W. H., Chakrabarty, R. K., Hasheminassab, S., and Diner, D. J.: Black carbon emissions generally underestimated in the global south as revealed by globally distributed measurements, Nature communications, 16, 7010, 2025.

Rosenfeld, D., Lohmann, U., Raga, G., O'Dowd, C., Kulmala, M., Fuzzi, S., Reissell, A., and Andreae, M.: Flood or drought: How do aerosols affect precipitation?, Science, 321, 1309-1313, 10.1126/science.1160606, 2008.

Ryder, C. L., Highwood, E. J., Lai, T. M., Sodemann, H., and Marsham, J. H.: Impact of atmospheric transport on the evolution of microphysical and optical properties of Saharan dust, Geophysical Research Letters, 40, 2433-2438, 2013.

https://doi.org/10.5194/egusphere-2026-1299
Preprint. Discussion started: 13 March 2026

Salvador, P., Pey, J., Pérez, N., Querol, X., and Artíñano, B.: Increasing atmospheric dust transport towards the western Mediterranean over 1948–2020, NPJ Climate and Atmospheric Science, 5, 34, 2022.

Salvador, P., Alonso-Pérez, S., Pey, J., Artíñano, B., De Bustos, J. J., Alastuey, A., and Querol, X.: African dust outbreaks over the western Mediterranean Basin: 11-year characterization of atmospheric circulation patterns and dust source areas, Atmospheric Chemistry and Physics, 14, 6759-6775, 2014.

Samset, B. H., Stjern, C. W., Andrews, E., Kahn, R. A., Myhre, G., Schulz, M., and Schuster, G. L.: Aerosol absorption: Progress towards global and regional constraints, Current climate change reports, 4, 65-83, 2018.

Scarnato, B. V., China, S., Nielsen, K., and Mazzoleni, C.: Perturbations of the optical properties of mineral dust particles by mixing with black carbon: a numerical simulation study, Atmospheric Chemistry and Physics, 15, 6913-6928, 2015.

Schwikowski, M., Seibert, P., Baltensperger, U., and Gaggeler, H. W.: A study of an outstanding Saharan dust event at the high-alpine site Jungfraujoch, Switzerland, Atmospheric Environment, 29, 1829-1842, https://doi.org/10.1016/1352-2310(95)00060-C, 1995.

Seinfeld, J. H., Bretherton, C., Carslaw, K. S., Coe, H., DeMott, P. J., Dunlea, E. J., Feingold, G., Ghan, S., Guenther, A. B., Kahn, R., Kraucunas, I., Kreidenweis, S. M., Molina, M. J., Nenes, A., Penner, J. E., Prather, K. A., Ramanathan, V., Ramaswamy, V., Rasch, P. J., ..., and Wood, R.: Improving our fundamental understanding of the role of aerosol−cloud interactions in the climate system, Proceedings of the National Academy of Sciences, 113, 5781-5790, 10.1073/pnas.1514043113, 2016.

Sellegri, K., Laj, P., Venzac, H., Boulon, J., Picard, D., Villani, P., Bonasoni, P., Marinoni, A., Cristofanelli, P., and Vuillermoz, E.: Seasonal variations of aerosol size distributions based on long-term measurements at the high altitude Himalayan site of Nepal Climate Observatory-Pyramid (5079 m), Nepal, Atmos. Chem. Phys., 10, 10679-10690, 10.5194/acp-10-10679-2010, 2010.

Shaw, G. E.: Aerosols at a mountaintop observatory in Arizona, Journal of Geophysical Research: Atmospheres, 112, 2007.

Sigmund, A., Freier, K., Rehm, T., Ries, L., Schunk, C., Menzel, A., and Thomas, C. K.: Multivariate statistical air mass classification for the high-alpine observatory at the Zugspitze Mountain, Germany, Atmospheric Chemistry and Physics, 19, 12477-12494, 2019.

Singh, A., Chou, C. C. K., Chang, S.-Y., Chang, S.-C., Lin, N.-H., Chuang, M.-T., Pani, S. K., Chi, K. H., Huang, C.-H., and Lee, C.-T.: Long-term (2003–2018) trends in aerosol chemical components at a high-altitude background station in the western North Pacific: impact of long-range transport from continental Asia, Environmental Pollution, 265, 114813, 2020.

Skiles, S. M., Flanner, M., Cook, J. M., Dumont, M., and Painter, T. H.: Radiative forcing by light-absorbing particles in snow, Nature Climate Change, 8, 964-971, 10.1038/s41558-018-0296-5, 2018.

Song, Q., Zhang, Z., Yu, H., Ginoux, P., and Shen, J.: Global dust optical depth climatology derived from CALIOP and MODIS aerosol retrievals on decadal timescales: regional and interannual variability, Atmos. Chem. Phys., 21, 13369-13395, 10.5194/acp-21-13369-2021, 2021.

Sprenger, M. and Wernli, H.: The LAGRANTO Lagrangian analysis tool - version 2.0, Geoscientific Model Development, 8, 2569-2586, 10.5194/gmd-8-2569-2015, 2015.

Sun, Y. L., Wang, Z. F., Du, W., Zhang, Q., Wang, Q. Q., Fu, P. Q., Pan, X. L., Li, J., Jayne, J., and Worsnop, D. R.: Long-term real-time measurements of aerosol particle composition in Beijing, China: seasonal variations, meteorological effects, and source analysis, Atmos. Chem. Phys., 15, 10149-10165, 10.5194/acp-15-10149-2015, 2015.

https://doi.org/10.5194/egusphere-2026-1299
Preprint. Discussion started: 13 March 2026

Tositti, L., Riccio, A., Sandrini, S., Brattich, E., Baldacci, D., Parmeggiani, S., Cristofanelli, P., and Bonasoni, P.: Short-term climatology of PM10 at a high altitude background station in southern Europe, Atmospheric Environment, 65, 142-152, https://doi.org/10.1016/j.atmosenv.2012.10.051, 2013.

Tositti, L., Brattich, E., Cassardo, C., Morozzi, P., Bracci, A., Marinoni, A., Di Sabatino, S., Porcù, F., and Zappi, A.: Development and evolution of an anomalous Asian dust event across Europe in March 2020, Atmospheric Chemistry and Physics, 22, 4047-4073, 2022.

Vogel, F., Putero, D., Bonasoni, P., Cristofanelli, P., Zanatta, M., and Marinoni, A.: Saharan dust transport event characterization in the Mediterranean atmosphere using 21 years of in-situ observations, Atmos. Chem. Phys., 25, 15453-15468, 10.5194/acp-25-15453-2025, 2025.

Wernli, H.: A Lagrangian-based analysis of extratropical cyclones. II: A detailed case-study, Quarterly Journal of the Royal Meteorological Society, 123, 1677-1706, https://doi.org/10.1002/qj.49712354211, 1997.

Wilcox, E. M., Thomas, R. M., Praveen, P. S., Pistone, K., Bender, F. A. M., and Ramanathan, V.: Black carbon solar absorption suppresses turbulence in the atmospheric boundary layer, Proceedings of the National Academy of Sciences, 113, 11794-11799, 2016.

Williams, J., De Reus, M., Krejci, R., Fischer, H., and Ström, J.: Application of the variability-size relationship to atmospheric aerosol studies: estimating aerosol lifetimes and ages, Atmospheric Chemistry and Physics, 2, 133-145, 2002.

Wittmaack, K.: Advanced evaluation of size-differential distributions of aerosol particles, Journal of Aerosol Science, 33, 1009-1025, 2002.

WMO: Airborne Dust Bulletin, 2023.

Xu, J., Wang, Z., Yu, G., Sun, W., Qin, X., Ren, J., and Qin, D.: Seasonal and diurnal variations in aerosol concentrations at a high-altitude site on the northern boundary of Qinghai-Xizang Plateau, Atmospheric research, 120, 240-248, 2013.

Yadav, A. C., Tatarov, B., Song, R., Ghita, A., and Müller, D.: Characterizing the Saharan dust transported to the UK through lidar ratio, particle depolarization, and spectroscopic measurements, Atmospheric Environment, 121613, 2025.

Zardi, D. and Whiteman, C. D.: Diurnal mountain wind systems, Mountain weather research and forecasting: Recent progress and current challenges, 35-119, 2012.